World Journal of Cancer and Oncology Research, 2023, 2, 592
www.scipublications.org/journal/index.php/wjcor
DOI: 10.31586/wjcor.2023.592

Seminar in writing

Novel nano-thermal ablation therapy using functionalized heat-generating nanoparticles for solid cancer treatment

Tomio Morino [1,*], Noriyasu Kawai [1], Akira Ito [2], Takeshi Kobayashi [3], Takahiro Yasui [1]

[1] Department of Nephro-urology, Nagoya City University Graduate School of Medical Sciences, 1 Kawasumi, Mizuho-cho, Mizuho-ku, Nagoya 467-8601, Japan

[2] Department of Chemical Systems Engineering, School of Engineering, Nagoya University, Furo-cho, Chikusa-ku, Nagoya 464-8603, Japan

[3] Emeritus professor, School of Engineering, Nagoya University, Furo-cho, Chikusa-ku, Nagoya 464-8603, Japan

[*] Correspondence: Tomio Morino (t-morino@med.nagoya-cu.ac.jp)

Abstract: This seminar in writing introduced novel cancer thermal therapy using functionalized heat-generating nanoparticles with about 100 nm diameter, administered via intratumor injection. The nanoparticles named magnetites cationic lipid composite particles (MCL particles) were composed of about 10 nm magnetites (Fe_3O_4), a cationic lipid and two neutral lipids. Magnetites in MCL particles generated heat due to external alternating magnetic field (AMF) irradiation to kill cancer cells nearby located. A cationic lipid component conferred several functions to MCL particles necessary for its efficacy and safety. Origination of the therapy with MCL particles was summarized by referring to our earlier reports in 1996-2014. Further characterizations of MCP particles and utility of heat dose index for treatment control were summarized by referring to our recent reports in 2019-2022. Unpublished data were supplemented to support overall understanding of the therapy. Purpose of this seminar is to clarify novel principle of the therapy in comparison with conventional thermal therapies and to discuss its clinical application.

Keywords: MCL particles; cell adhesion; intratumor injection; alternating magnetic field; occlusive embolus induction; heat dose index; nanoparticle filtration, nano-thermal ablation

How to cite this paper:

Morino, T., Kawai, N., Ito, A., Kobayashi, T., & Yasui, T. (2023). Novel nano-thermal ablation therapy using functionalized heat-generating nanoparticles for solid cancer treatment. *World Journal of Cancer and Oncology Research*, *2*(1), 29–46. Retrieved from https://www.scipublications.com/journal/index.php/wjcor/article/view/592

Received: December 25, 2022
Accepted: February 1, 2023
Published: February 4, 2023

1. Historical background of cancer thermal therapy

From around 1970s medical devices for cancer therapy to heat tumor region has been developed by means of external energy irradiation through body surface. Devices using radiofrequency capacitance [1, 2], annular phased microwave array [3] and high intensity focused ultrasound [4] have been clinically applied, however inevitable heating of surrounding normal tissues and irradiated body surface seemed to be not always settled even today (**Figure 1a**).

An idea to overcome this fundamental issue had been proposed in advance in 1950s by Gilchrist et al in Luke's hospital, Chicago, in Illinois. He showed accumulation of micrometer-scale ferrite materials in lymph nodes *in vivo* and proposed to kill node-metastasized cells by material's heat generation induced by external alternating magnetic field (AMF) irradiation [5, 6]. Although his target was not proved so far, his idea to use heat-generating materials has been realized by millimeter- to centimeter-scale implants fixed in tumor tissue. Needle shaped insertion implant [7], cylinder shaped embedding implant [8] and bone cavity applied cement implant [9] have been clinically applied with appropriate energy irradiation, and obvious ablation of contacting tumor tissue has been proved (**Figure 1b, upper**). Action of these heat-generating implants was similar to that

of radiofrequency ablation (RFA) therapy with percutaneously inserted heat-generating tip [10] (**Figure 1b, lower**).

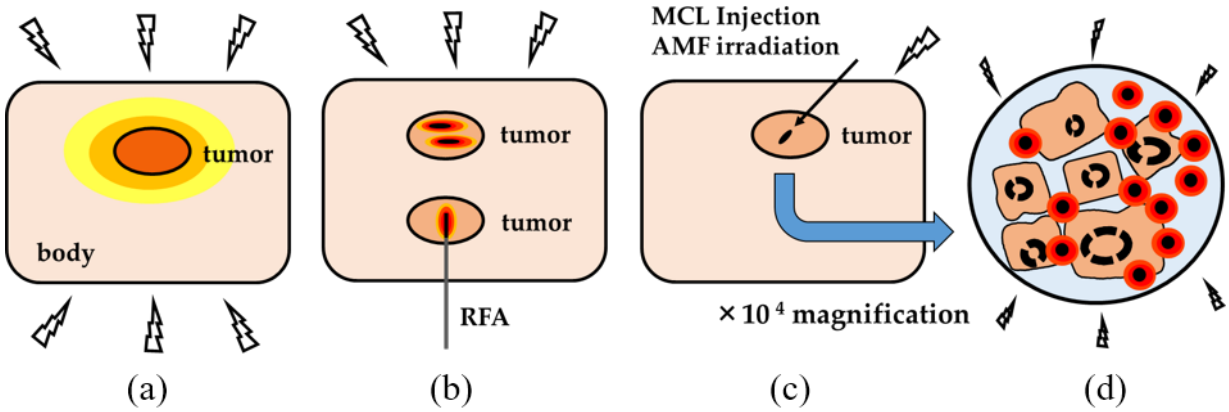

Figure 1. Principles of cancer thermal therapies

Temperature increase in the therapy were illustrated with temperature gradient from low (yellow) to high (red). External energy irradiation was shown by waved arrows. (a) Tumor region in a body was heated by external energy irradiation such as radiofrequency wave, microwave or ultrasound; (b) (upper) Heat generation of implanted materials in tumor was induced by external energy irradiation; (lower) Heat generation of inserted needle tip in tumor was induced electronically in radiofrequency ablation therapy; (c) MCL particles were injected intratumor, and heat generation of MCL particles was induced by external AMF irradiation; (d) Heat generation of MCL particles was illustrated under 10^4 magnifications.

2. Potentiality of heat-generating nano-magnetites as thermal device

In 1979 Gordon et al in Illinois showed downsized 6 nm magnetites (Fe_3O_4) were phagocytosed by cancer cells *in vivo*. He observed the cells were killed by magnetites' heat generation induced by external AMF irradiation with little effect on surrounding normal cells [11]. He proposed novel concept of intracellular hyperthermia and suggested importance of biophysical properties of nano-magnetites for efficacy enhancement. Since he had to administer submicron aggregates of 6 nm magnetites, following studies seemed to seek colloidal magnetites suspension for medical use. Aminosilan-modified magnetites [12], dextran-modified magnetites [13], polyethylene glycol modified magnetites [14] were successfully prepared in colloid. Notably, these modifications resulted in pharmacokinetic changes of core magnetites such as increased cellular uptake and decreased cellular degradation [12], prolonged blood circulation [13] and enhanced distribution in tumor stroma [14]. As Gordon's suggestion, biophysical modulation has become a potent approach to functionalize nano-materials satisfactory to medical needs.

3. Origination and characterization of magnetites cationic lipid composite particles (MCL particles)

In 1996 Japanese researchers in Nagaya reported another type of colloidal nanoparticles composed of nanometer-scale magnetites, a cationic lipid and two neutral lipids [15]. The nanoparticles were injected intratumor, and its heat generation was induced by AMF irradiation around 100 kHz. Interestingly, *in vivo* anticancer activity was drastically enhanced by repeated AMF irradiations with 1-day intervals. Then, multiple irradiations protocol for cancer treatment was constructed on a basis of temperature monitoring, and complete tumor regressions were frequently observed in several animal

tumor models [16-21]. Clinical research has been conducted preliminary, and its results was briefly shown [22] (p.1721).

Recently, structure and functions of the nanoparticles were investigated in detail and its therapeutic use was refined [23-27]. Optimum size of magnetites for heat generation under 100 kHz AMF was shown about 10 nm [23] (**Figure 2a**). Electron microscopic observation of the nanoparticles revealed composite structure of magnetites and three lipids with averagely 25 magnetites containment and 107.1 nm diameter (**Figure 2b**). Then, the former name of magnetite cationic liposomes [15] was revised to magnetite cationic lipid composite particles (MCL particles) [24]. Roles of lipid components, especially a cationic lipid, were shown significant to confer several functions such as cell-adhesion activity [24], *in vivo* mobility within tumor tissue [25], tumor blood vessel disruption activity and none infiltration property toward surrounding normal tissue (**unpublished result**). Furthermore, theoretical background of treatment designing was constructed with heat dose index, and its advantage against temperature index was shown [26, 27]. Principle of the therapy with MCL particles was illustrated under magnification (**Figure 1c,d**).

In the following chapters, the therapy was overviewed, and its difference from conventional thermal therapies were clarified (**Figure 1**). Future prospectus for clinical application was discussed finally.

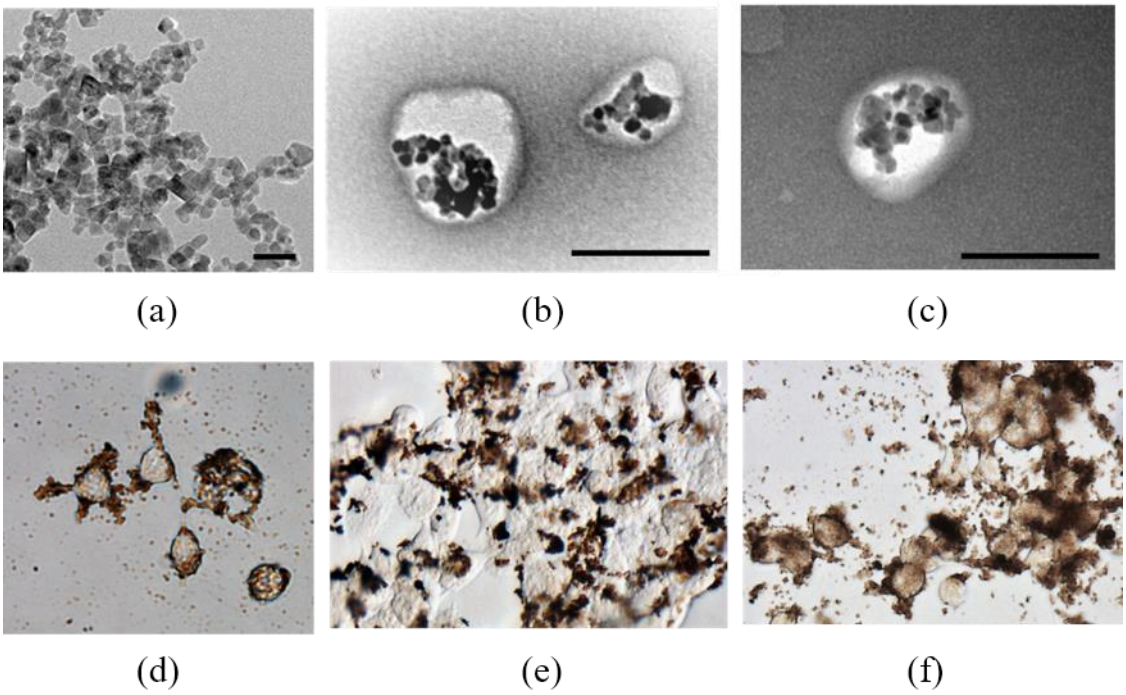

Figure 2. Composite structure and cell-adhesion mediated cytotoxicity of MCL particles

MCL particles were prepared with magnetites, a cationic lipid and two neutral lipids by sonication [15] and observed by electron microscopy [24]. Human prostate cancer LNCaP cells were exposed to excess amount of MCL particles and washed before microscopic observation and AMF irradiation at 100 kHz for 30 min [24].

(**a**) Magnetites used for MCL particles preparation. Scale 30 nm; (**b**) MCL particles prepared. Scale 100 nm; (**c**) MCL particles released from cancer cell membrane after AMF irradiation. Scale 100 nm; (**d**) Adhesion of MCL particles to isolated cancer cells; (**e**) Adhesion of MCL particles to semi-confluent cancer cells; (**f**) Morphological change of semi-confluent cancer cells and releasing of MCL particles after AMF irradiation.

3.1. Cell-adhesion and heat-generation mediated cytotoxicity of MCL particles

MCL particles have been designed to adsorb negatively-charged cancer cells membrane by positive charge conferred by a cationic lipid component [15] and was recently shown to have positive zeta potential of + 48.9 mV [24]. Adhesion of MCL particles to isolated or semi-confluent cancer cells were confirmed by microscopic observation (**Figure 2d,e**). By AMF irradiation, morphological change of adsorbed cells was immediately induced to spherical shape (**Figure 2f**). Bursting of cellular membrane was frequently observed by electron microscopy, and cellular death was confirmed by trypan blue extrusion assay [24]. On the other hand, nanoparticles lacking a cationic lipid component showed negative zeta potential and less cell adhesion activity and cytotoxicity [15, 24]. Two neutral lipid components were shown essential to form and maintain composite structure (**unpublished data**).

During AMF irradiation, releasing of MCL particles to culture medium was observed (**Figure 2f**), likely due to declined electrostatic interaction with dying cells' membrane. However, structural change of released MCL particles was not observed by electron microscopy (**Figure 2c**). Increase of medium temperature was not observed during AMF irradiation because of minute local heating on cell membrane [24], as reported with other type of cell-adhesive heat-generating nanoparticles by Creixell et al in 2011 [28]. Cytotoxicity of MCL particles was represented by Creixell's method using heating value of Joule (J) [28] and was shown 1.2×10^{-4} J/cell under semi-confluent condition [24].

3.2. Induction of tumor necrosed area in vivo in the area where MCL particles distributed

Complete tumor regressions have been observed under multiple irradiations protocol with 1 days [16-21]. Histological study has been conducted with tumors dissected after injection, once irradiation, twice irradiations and thrice irradiations [18]. MCL particles were observed in black without staining (**Figure 3a**), and induced tumor necrosed area was observed in pink with hematoxylin eosin (HE) staining (**Figure 3b**). Notably, necrosed area was observed to overlap the area where MCL particles distributed in every tumor. Tumor necrosis induction *in vivo* was well consistent with cell-adhesion mediated cytotoxicity shown *in vitro*.

Recently, boundary region between necrosed and alive areas was observed microscopically with mouse B16 melanoma [25]. By enlarging boundary region, tumor necrosed area was confirmed by HE staining in pink (**Figure 4a,b,c**). Necrosed tumor cells were observed to contact directly with alive tumor cells stained in faint blue, and cells with intermediate morphological features was not observed around the boundary (**Figure 4c**). Therefore, cellular necrosis induction was considered strictly dependent on cell-adhesion even *in vivo*, and heat transfer from MCL particles-distributed area was not cytotoxic against neighboring cells (**Figure 3,4c**). This cytotoxic profile *in vivo* was same as Gordon' observation of little effect on surrounding cells in intracellular hyperthermia [11] (p.91, 93) because of local minute heating of nanoparticles in cytoplasm [11] or on cell membrane [24, 28].

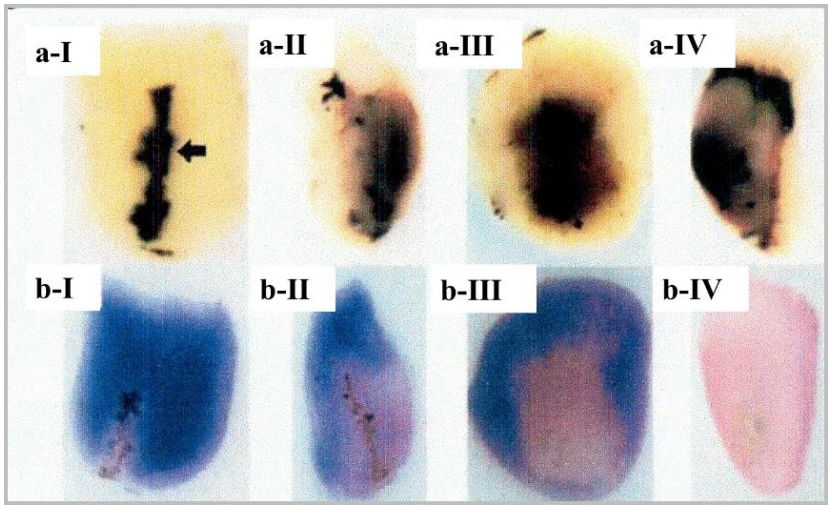

Figure 3. Tumor necrosis induction in MCL particles-distributed area and its expansion by multiple irradiations

MCL particles of 5.17 mg were injected with syringe pump to subcutaneously transplanted T-9 rat glioma (10 mm diameter). Injection amount of 5.17 mg MCL particles was achieved by 0.4 ml injection of 12.9 mg-MCL/ml liquid formulation. Tumors were irradiated for 30 min once, twice, or thrice with 1-day intervals. In this study, treatment was controlled with temperature index to keep skin temperature on tumor around 45 ℃ by stepwise changing of irradiator output. Magnetic flux density at tumor locus was not constant but controlled more than 15 mT. Each tumor was dissected after irradiation, and two side by side paraffine sections were observed without staining (**a**) and with hematoxylin eosin (HE) staining (**b**). Through the courtesy of Springer-Verlag, data was cited from reference [18].

(**-I**) After injection; (**-II**) After 1st irradiation; (**-III**) After 2nd irradiation; (**-IV**) After 3rd irradiation. Necrosed and alive tumor areas were observed in pink and blue respectively. In this case, whole tumor necrosis was achieved by thrice irradiations.

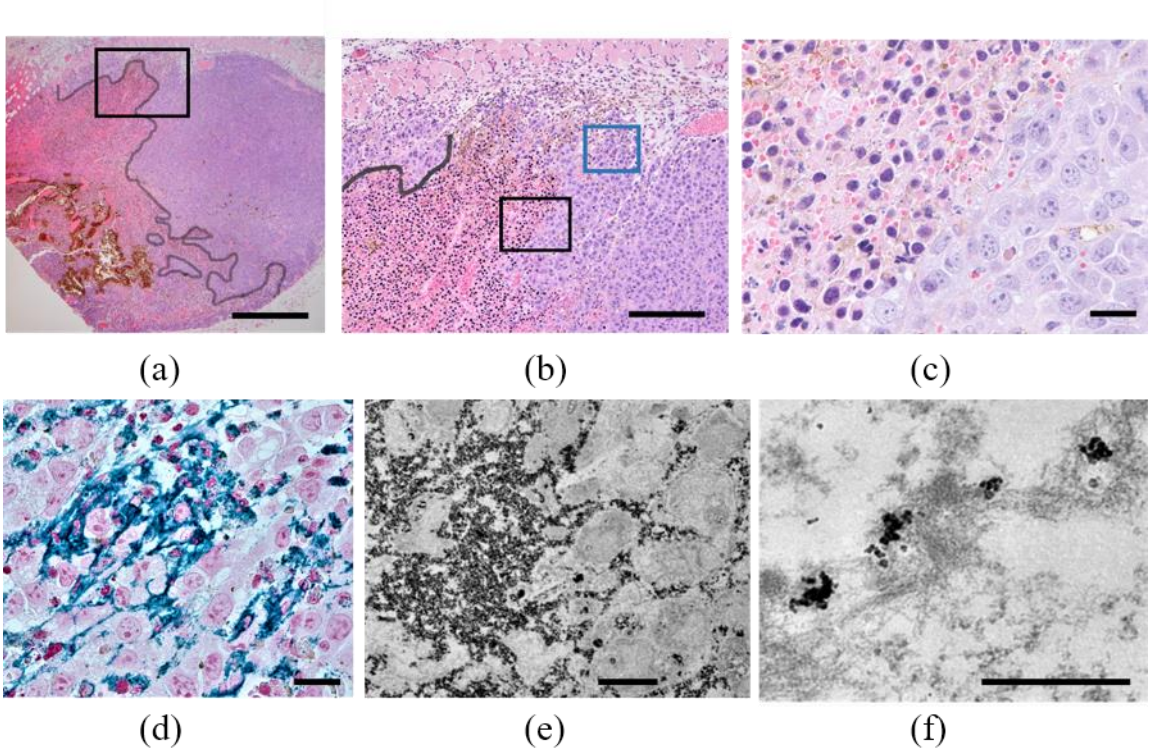

Figure 4. Direct contacting of necrosed and alive tumor cells and movement of MCL particles to neighbor alive area

MCL particles of 7.5 mg were injected to edge of mouse B16 melanoma (11 mm diameter) in order to construct partially necrosed tumor sample. Injection amount of 7.5 mg MCL particles was achieved by 0.1 ml injection of 75 mg-MCL/ml liquid formulation. Tumors were applied to 30 min AMF irradiation at 15 mT and dissected 1 day after the irradiation. Dissected tumor was divided two blocks in the middle. One block was applied to prepare paraffine sections parallel to dividing surface, and two side by side sections were stained by HE (**a-c**) and BB (**d**). Another block was solidified in epoxy resin, and sections parallel to dividing surface were used for electron microscopic observation. Observation area was optically checked prior to uranium acetate staining for sample preparation (**e,f**). Outline of tumor necrosed area was indicated with drawn line [25].

(**a**) Induction of tumor necrosed area stained in pink. Scale 1 mm; (**b**) Enlargement of black square region in **a**. Scale 0.5 mm; (**c**) Enlargement of black square region in **b**. Necrosed cells in pink were contacting directly to alive cells in faint blue. Scale 20 μm; (**d**) Observation of MCL particles stained in dense blue. MCL particles were localized among alive tumor cells. The area corresponded to blue square region in **b**. Scale 20 μm; (**e**) MCL particles observed among alive tumor cells. Scale 10 μm; (**f**) MCL particles observed in interstitial space of alive tumor cells. Scale 500 nm.

3.3. Mobility of MCL particles to neighbor tumor alive area for necrosis expansion

Expansion of MCL particles-distributed area by multiple irradiations was critical to induce whole tumor necrosis (**Figure 3-IV**). Recently, process of MCL particles expansion was investigated with tumors dissected just before the 2nd irradiation, namely 24 hours after the 1st irradiation [25]. One of two side by side sections were stained by Berlin blue (BB) in order to observe MCL particles. MCL particles stained in dense blue were observed among alive tumor cells stained in faint red by BB (**Figure 4d**) which corresponded to alive tumor cells stained in faint blue by HE (**Figure 4b**). Distribution of MCL particles among alive tumor cells were also confirmed by electron microscopy (**Figure 4e**). Data

verified necessity of irradiation intervals in multiple irradiation protocol to allow movement of MCL particles to neighbor alive area. Furthermore, stability of composite structure of MCL particles was shown by maintenance of magnetites containment observed among interstitial space of alive cells (**Figure 4f**). Structural stability of MCL particles shown *in vivo* and *in vitro* (**Figure 2c**) supported reusage of MCL particles in multiple irradiation protocol. On the other hand, significance of lipid components for structural maintenance was paradoxically implied by carboxydextran-modified heat-generating maghemite (γ-Fe_2O_3), which was converted to millimeter-scale massive aggregate by AMF irradiation and showed less anticancer activity in this usage [29] (p.29).

Driving forces of mobility of MCL particles has been discussed [25] with hydraulic conductivity caused by injection of liquid formulation [30], lymphatic fluid flow in tumor tissue [31], electrostatic attraction of alive tumor cells toward positively-charged MCL particles in Brownian motion [24] (p.28). It is notable that MCL particles sized around 100 nm are susceptible to these driving forces and able to move interstitial space of tumor tissue (**Figure 4e,f**).

3.4. Tumor blood vessel disruption and occlusive embolus induction

Action against tumor blood vessels *in vivo* was revealed recently in our laboratories (**unpublished result**). In untreated tumor, tumor blood vessels with intact biconcave erythrocytes were observed by optical and electron microscopy (**Figure 5a**,**d**). In treated tumor, serious erythrocytes leakage was observed in necrosed area stained in pink, and leakage sites on the vessels were occasionally observed (**Figure 5b,c**). Simultaneously, serious tumor tissue destruction was observed in all of necrosed area by optical and electron microscopy (**Figure 5b,c,e**). Erythrocytes leakage could be occurred at fragile sites of irregular tumor blood vessel structure [32] due to lacked vessel-supporting function of tumor tissue and/or necrosis induction of wall cell, pericyte (**Figure 5e**). Interestingly, thrombotic occlusive embolization induced by hemostasis response was observed by electron microscopy in all of tumor blood vessels found in necrosed area (**Figure 5e,f,g**).

It was well known that stasis of tumor blood flow by embolization caused anticancer activity owing to nutrient and oxygen starvation [33]. From the beginning of this research, complete tumor regressions have been frequently observed in all of tested tumor models [21] (p.121), [26, 27]. To elucidate the efficacy, actions other than necrosed area induction have been searched in our laboratories, and anticancer immunity accelerated by Hsp70 expression and tumor antigen exposure has been reported [18,34]. At this late day, tumor cell starvation caused by newly-found embolus induction was considered to participate in total anticancer activity reported.

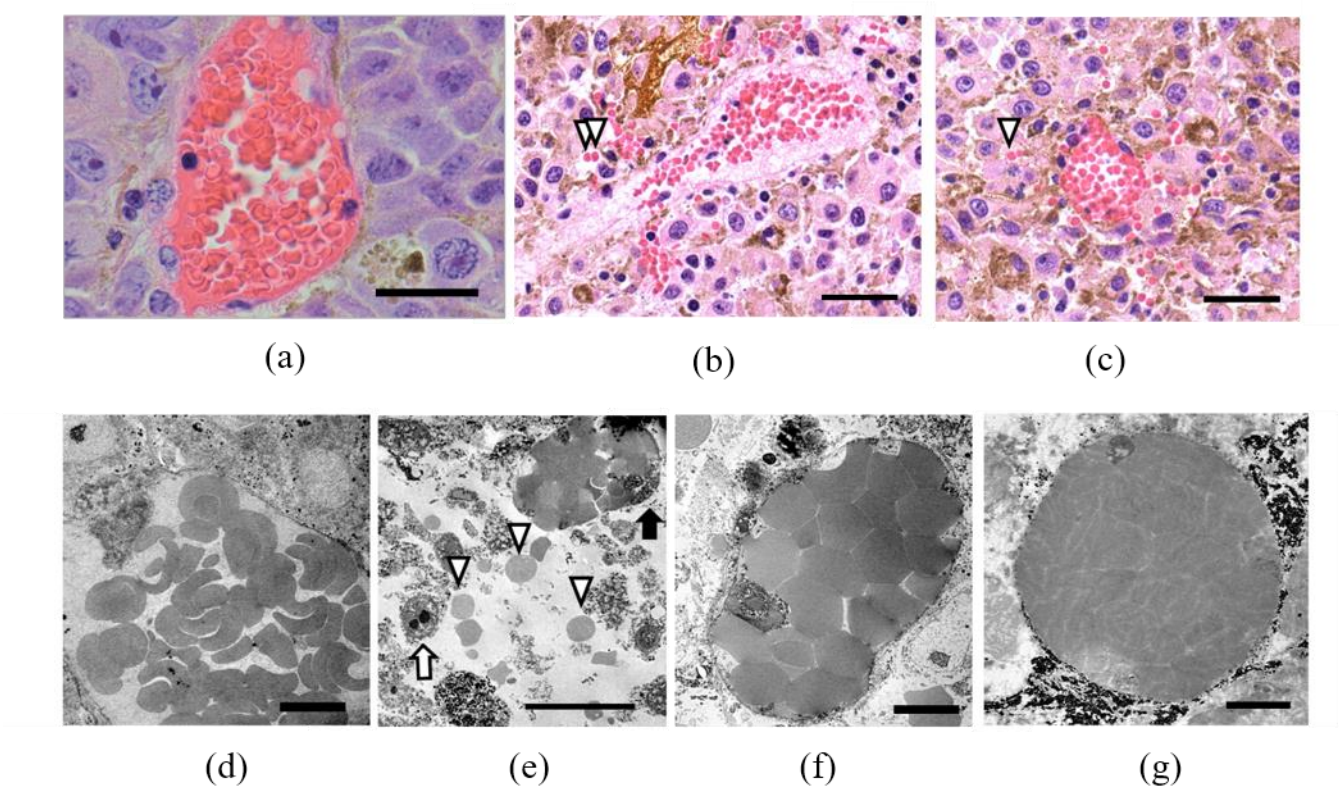

Figure 5. Tumor blood vessel disruption and thrombotic embolus induction

MCL particles of 15 mg were injected to center of mouse B16 melanoma (11 mm diameter) in order to construct widely necrosed tumor sample. Injection amount of 15 mg MCL particles was achieved by 0.2 ml injection of 75 mg-MCL/ml liquid formulation. Tumors were applied to 30 min AMF irradiation at 15 mT and dissected 1 day after the irradiation. Tumor sections were prepared as Figure 4 and applied to HE staining (**a-c**) and electron microscopic observation (**d-g**). Leaked erythrocytes were indicated by arrowhead. Necrosed tumor cells and pericyte on blood vessel were indicated by white and black arrows, respectively (**unpublished result**).

(**a**) Tumor blood vessels of untreated tumor. Scale 20 μm; (**b,c**) Erythrocytes leakage from tumor blood vessels of treated tumor. Scale 20 μm; (**d**) Tumor blood vessel of untreated tumor. Scale 10 μm; (**e**) Observation of tumor tissue destruction, erythrocyte leakage and embolus induction in tumor blood vessel. Scale 10 μm; (**f,g**) Observation of two types of thrombotic embolus with flat or wrinkled erythrocytes. Scale 10 μm.

3.5. Absence of histological alteration in surrounding normal tissue

Injury induction of surrounding normal tissue was not observed in all of histological studies of animal tumor models [16-18,25,35] and human tumors [22] (p.1721), and was pointed out in a few reports [17] (p.148), [22]. In detail observation of normal tissue was recently reinvestigated in our laboratory (**unpublished result**). In subcutaneously transplanted tumor models, normal fat cell layer was observed next to tumor tissue stained in faint blue, and normal blood vessels with intact erythrocytes were observed among fat cell layer (**Figure 6a**). Then, tumor samples in which necrosis was fully induced to tumor edge were constructed for normal tissue observation, and a typical specimen was shown (**Figure 6b**). Normal blood vessel was found in proximity to necrosed tumor tissue, but histological alternation was not observed and intact biconcave erythrocytes were confirmed in the vessel (**Figure 6c**). Not limited to this specimen, histological alterations

were not observed in all of normal blood vessels and fat cell layer near necrosed tumor tissue.

On contrary, tumor blood vessels found in necrosed area in pink showed serious disorders (**Figure 6d**).

Infiltration of MCL particles toward surrounding normal tissues was not observed in all of histological studies reported [16-18, 22, 25, 35], and was pointed out in a report [25]. Accumulation of MCL particles at boundary between normal tissue was shown in mouse osteosarcoma model [35] (p.583) and mouse melanoma model (**Figure 6e**). Therefore, histological integrity of normal tissue was considered to be explained by some barrier function against MCL particles infiltration at the boundary.

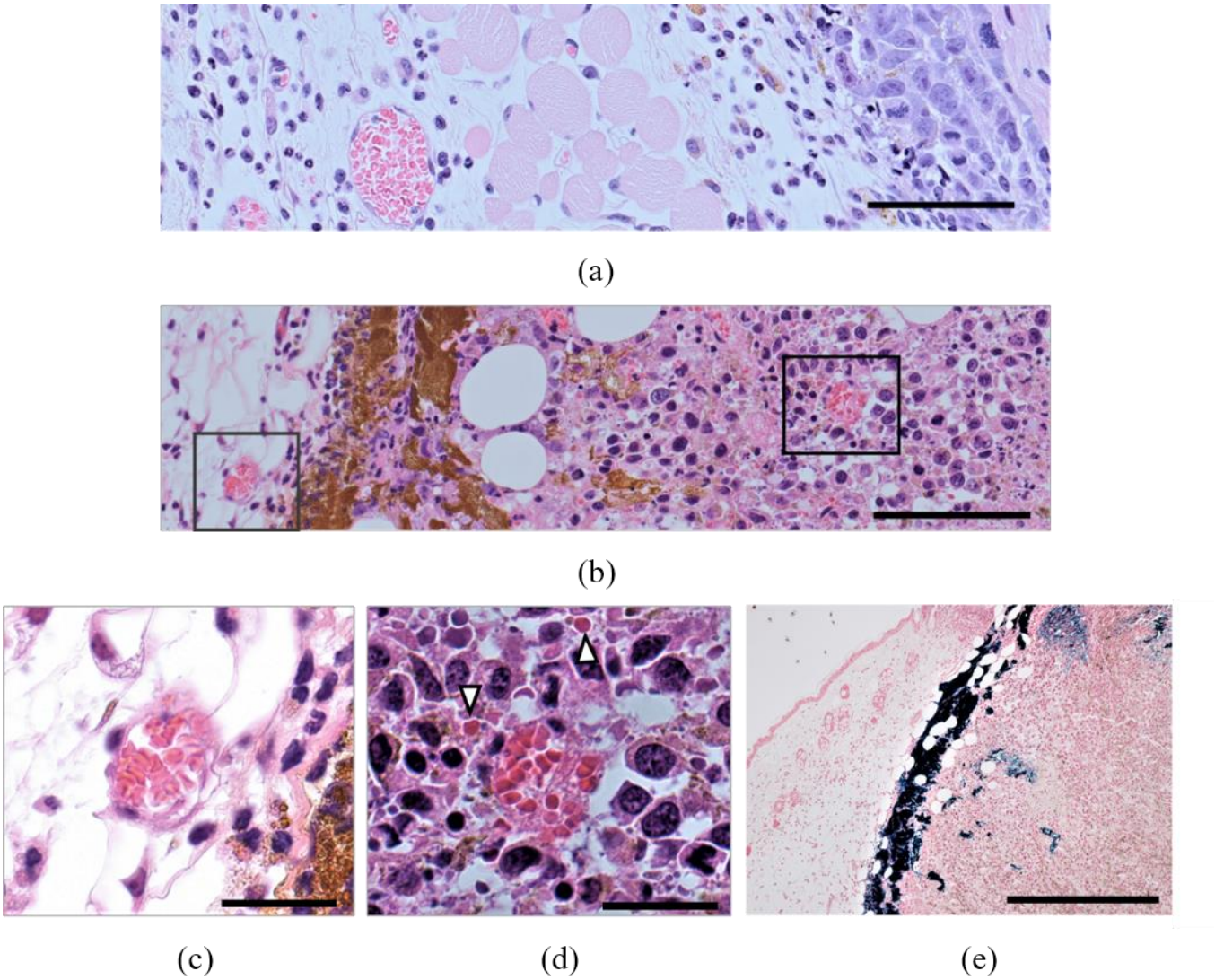

Figure 6. Absence of histological alteration of surrounding normal tissue and none infiltration of MCL particles

Widely necrosed tumor sample was construct as Figure 5. Tumor sections were stained by HE (**a-d**) and BB (**e**). Wide area of specimen was observed with Zen tiling method of Carl Zeiss (**a,b**). Boundary region between normal and tumor tissues of **b** corresponded to that of **e** (**unpublished result**).

(**a**) Normal and tumor tissue of untreated tumor. Nucleus of normal fat cells were observed as dense spot in violet, and a few normal blood vessels were observed in normal

tissue. Scale 100 nm; (**b**) Normal and tumor tissue of treated tumor. Full tumor necrosis was confirmed by HE staining in pink. Blood vessels found in normal and tumor tissue were indicated by black squares. Scale 100 μm; (**c**) Enlargement of normal blood vessel observed in **b**. Scale 20 μm; (**d**) Enlargement of tumor blood vessel observed in **b**. Scale 20 μm; (**e**) Accumulation of MCL particles at boundary between normal tissue. MCL particles were stained in dense blue. Scale 50 μm.

3.6. Possible mechanism of MCL particles filtration at boundary between normal tissue

Macromolecules and nanoparticles have been shown to be retained in tumor tissue without lymphatic clearance, and novel concept of cancer macromolecular therapy has been proposed by Matsumura et al in 1986 [36]. This finding has implied limited nanoparticle penetration to normal tissue in general. On the other hand, basement membrane like structure has been observed at the boundary in human hepatocarcinoma [37] and mouse B16 melanoma used in our laboratory (**unpublished result**). It was well known that basement membrane had barrier function against substance penetration in size and charge dependent manner [38-41].

Recently in order to investigate mechanism of none infiltration of MCL particles, unmodified magnetites was applied to the treatment in our laboratory (**unpublished result**). Infiltration of magnetites to surrounding normal tissue was obviously observed 1 day after injection (**Figure 7a**). Magnetites observed in tumor tissue 1 day after disappeared from whole tumor tissue 3 days after (**Figure 7b,c**). In surrounding normal tissue, erythrocytes leakage and fat cell nucleus disorder were seriously observed (**Figure 7d**). These results were quite different from of those of MCL particles such as retention in tumor tissue 3 days after (**Figure 3a-IV**), none infiltration to normal tissue (**Figure 6e**) and no injury induction of normal blood vessels and fat cells (**Figure 6c**).

Magnetites of about 10 nm was much smaller than MCL particles of averagely 107.1 nm diameter (**Figure 2a,b**). Zeta potential of magnetites in physiological pH 6.5 ~ 8.0 were + 8 ~ − 20 mV with isoelectric point of 6.8 (**unpublished result)**, whereas that of MCL particles was constantly around + 50 mV due to a cationic lipid component. Although further studies of boundary structure and its barrier function remained to be needed, MCL particles was shown to acquire none infiltration properties by composition with lipid components.

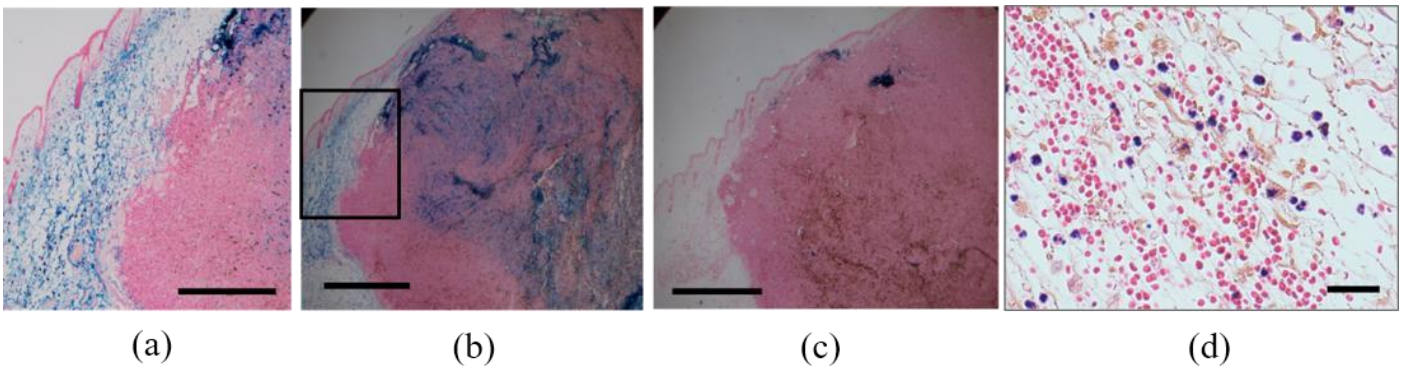

Figure 7. Infiltration of unmodified magnetites to surrounding normal tissue and induction of normal tissue disruption

Unmodified magnetites of 8.7 mg (corresponding to magnetites content in 15 mg MCL particles) were injected to center of mouse B16 melanoma (11 mm diameter). As Figure 5, tumors were applied to AMF irradiation once and dissected 1 day or 3 days after. Two side by sections were stained by BB (**a-c**) and HE (**d**) (**unpublished result**).

(**a**) Observation of magnetites infiltration to normal tissue 1 day after. Scale 0.5 mm; (**b**) Partial infiltration and retaining of magnetites in whole tumor tissue 1 day after. Black square region was shown in **a**. Scale 1 mm; (**c**); Disappearance of magnetites from whole tumor tissue 3 days after. Scale 1 mm; (**d**) Observation of surrounding normal tissue 1 day after. Serious erythrocyte leakage and fat cell nucleus disorder in dense violet were observed. Scale 20 μm.

4. Design and control of the treatment

When the treatment was controlled by skin temperature on transplanted tumors [16-21], anticancer activity has been shown to decrease in large tumor with 15 mm diameter [19]. Distribution of MCL particles in peripheral area of large tumor tended insufficient, even if skin temperature increase was achieved by heat transfer from heat generating area (**Figure 3**). In this therapy, tumor necrosis induction was delimited in MCL particles-distributed area, and heat transfer showed little effect on surrounding cells as discussed.

According to *in vitro* cytotoxicity represented by J/cell [24, 28] and thermal dose represented by J/cm^3 tumor volume [42-44] in the conventional thermal therapies [1,2], utility of heat dose index (J/cm^3 tumor volume) was investigated in order to construct theoretical background of treatment designing. Two medical devices of MCL particles and AMF irradiator were precisely tuned up, and heat generating activities of MCL particles (J/g-MCL · min) at tumor locus were measured parametrically with irradiator output. Then, heating value from injected MCL particles (J) was calculated by multiplication of three terms; heat generating activity (J/g-MCL · min) at tumor locus and irradiator output, injected amount of MCL particles (mg) and irradiation duration (min) [26].

4.1. Control of tumor necrosis induction with heat dose index

Heating value needed for complete regression was revealed recently by tracing treatment condition of small tumor (7 mm diameter) irradiated 30 min thrice with temperature index [21] (p.121). Skin temperature on mouse B16 melanoma (n=7, 7 mm, average 0.17 cm^3 tumor) was kept around 46 ℃ by stepwise changing of irradiator output, and heating values of each irradiation step was calculated based on heat generating activity (J/g-MCL · min) at each irradiator output. By summing up of each value, total heating value needed for complete regression of 0.17 cm^3 melanoma was shown 402.9 J in thrice total. By dividing with tumor volume, heat dose for complete regression was shown for the first time as 2,370 J/cm^3 tumor volume in thrice total [26].

Treatment condition of relatively large rat MAT-LyLu prostate tumors (n=10, 13 ~ 16 mm, 1.18 ~ 1.60 cm^3 tumor, average 1.36 cm^3 tumor) were designed based on benchmark of the heat dose, 2,370 J/cm^3 tumor volume in thrice total. Magnetic flux density of tumor locus was fixed to practical 15 mT (**unpublished result**), which brought heat generating activity of 768 J/g-MCL · min. Amount of MCL particles was fixed to high dose standard of 45 mg and was achieved by 0.2 ml injection of liquid formulation whose concentration was currently maximum 225 mg-MCL/ml. Irradiation was set as typical 30 min thrice condition. Mathematically, designed condition achieved heat doses of 2,122 ~ 2,862 J/cm^3 tumor volume in thrice total, as equivalent to benchmark. Under precisely controlled condition, complete regression of rat MAT-LyLu tumors were observed within 12 days after treatment [26]. Heating value needed for regression of 1.36 cm^3 tumor was increased to 3,111 J in thrice total due to tumor volume increase. The data showed utility of heat dose index (J/cm^3 tumor volume) in a range from small tumor (0.17 cm^3) to relatively large tumor (1.36 cm^3).

4.2. Design of much large tumor treatment with multiple site injections

Anticancer activity *in vivo* was based on stepwise necrosis expansion from an injection site (**Figure 3b, Figure 8a**). Therefore, number of injection sites and irradiation times of the therapy was theoretically variable (**Figure 8b,c**). In a case of very small tumor

of mouse B16 melanoma (n=10, 5~6 mm, average 0.09 cm^3 tumor), complete regression was achieved by twice irradiations as reported [21] (p.121) (**Figure 8c**).

In order to treat tumor larger than 1.36 cm^3 tumor, utility of multiple sites injections was recently investigated [27]. Much large 4 clonal tumors (2.19 ~ 3.81 cm^3 tumor) were induced by oral application of chemical carcinogen, 7,12-dimethylbenz[a]- anthracene (DMBA). Number of injection sites was designed 2 ~ 3 sites, and the high dose standard of 45 mg MCL particles was injected even space in order to expand necrosis from each injection site (**Figure 8b**). Feasibility of simultaneous injections with syringe pump was confirmed at the standard injection speed of 0.1 ml/10 min (**Figure 9a**). Irradiation was set as typical 30 min thrice condition at the standard 15 mT. Mathematically, designed treatment condition of 4 clonal tumors achieved heat doses of 1,965 ~ 2808 J/cm^3 tumor volume in thrice total, as equivalent to benchmark. Tumor regression were observed in getting dented fashion at day 2, namely just before the 2nd irradiation. Within 3 weeks, all tumors became undetected by palpation test after shaving (**Figure 9b,c**). Recurrence was not observed by 7 weeks after the regression, and efficacy of all tumors was evaluated as complete regression (**Figure 9d**) [27]. In general, large tumors were treated rather certainly than small, and efficacy was detected easily as denting in subcutaneously transplanted tumors.

Thus, multiple sites injection was practical for treatment of much large tumors and treatment condition was designed theoretically on a basis of heat dose index. As shown in **Figure 8**, schematic imaging of necrosis induction will be helpful for treatment design according to size and shape of target tumors.

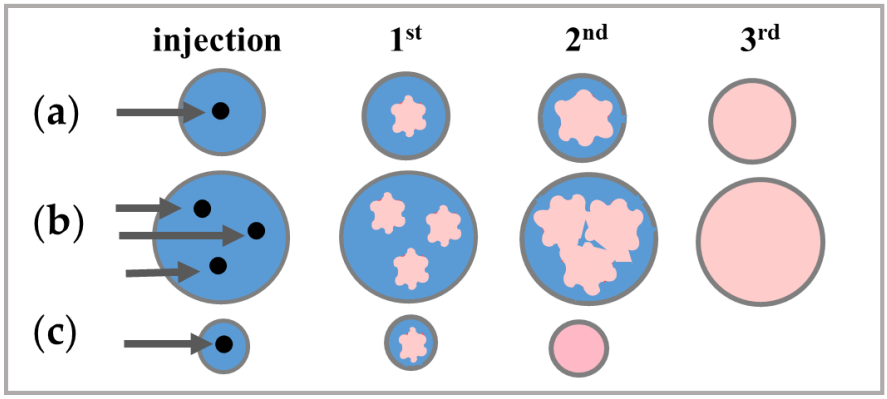

Figure 8. Scheme of necrosis area expansion to achieve whole tumor necrosis

Number of injection sites and irradiation times were designed according to tumor size. Injected MCL particles were shown in black and necrosed tumor area was shown in pink [27]. As tentatively described in the text, necrosis of 0.45 cm^3 tumor volume was induced from one injection site by once irradiation under the standard treatment condition which was specified by magnetic flux density; 15 mT, magnetic field frequency; 100 kHz, injected amount of MCL particles; 45 mg, irradiation duration; 30 min and generated heating value of 1,037 J in once alone.

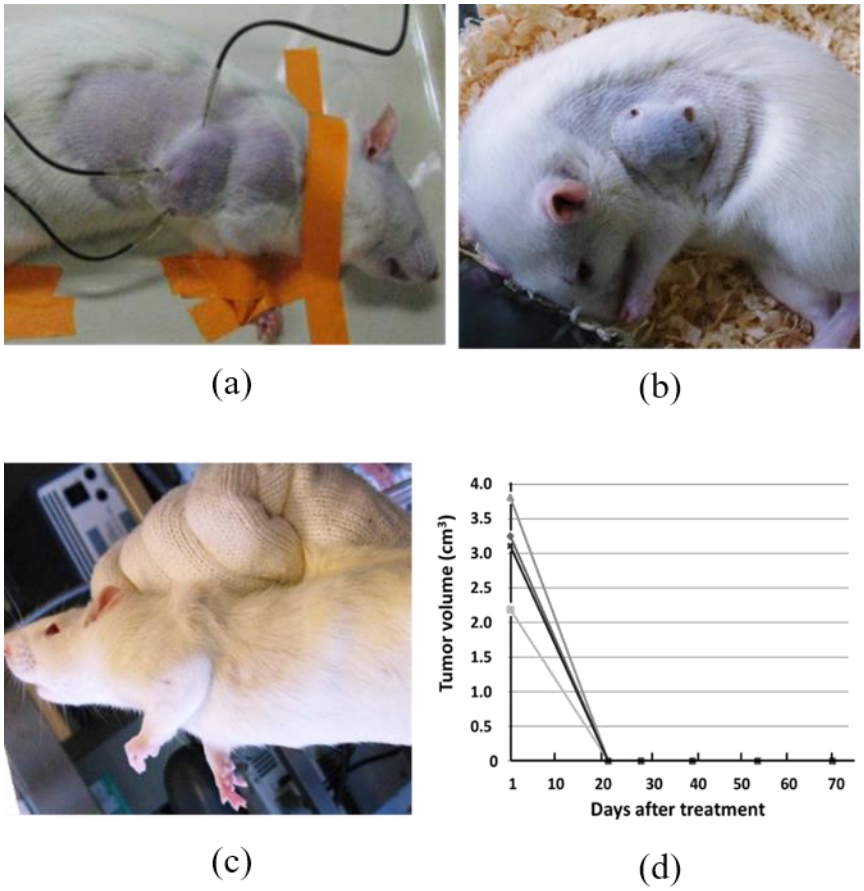

Figure 9. Treatment of much large tumors with multiple sites injection

DMBA of 20 mg was orally administered to Sprague-Dawley rats. Out of 80 rats, occurrence of mammary tumors was observed in 13 rats. Tumor volumes were confirmed to grow more than 25 cm^3 tumor volume with different growth speeds due to clonality. At 86 days after DMBA application, randomly selected 4 clonal tumors were applied to treatment of multiple sites injections. MCL particles of 45 mg were injected to each site at a speed of 0.1 ml/10 min with syringe pump. Injection amount of 45 mg MCL particles was achieved by 0.2 ml injection of 225 mg-MCL/ml liquid formulation. Tumors were treated under typical 30 min thrice condition at 15 mT. MCL particles was injected at day 1, and AMF was irradiated at day 1, 2, 3 [27].

(**a**) Simultaneous three site injections to much large tumor (18.2 mm × 21.8 mm, 3.81 cm^3 tumor); (**b**) Observation after two site injections to much large tumor (14.7 mm × 20.3 mm, 2.19 cm^3 tumor); (**c**) Complete regression of tumor in **b**; (**d**) Time course of tumor regression. Tumor volumes were shown only at initial and end points, because tumors regressed in getting dented fashion.

4.3. Unit efficacy of necrosed area induction under the standard and variant conditions

In this therapy there was concept of necrosed tumor volume (cm^3) from one injection site by once irradiation. It was regarded as unit efficacy of necrosis induction, and efficacy of multiple site injections and multiple time irradiations was regarded as result of piling-up of unit efficacies. An actual value of unit efficacy could be calculated from rat MAT-LyLu tumor experiment by following expression; 1.36 cm^3 necrosed tumor volume from one site by 3 irradiations using 3,111 J in thrice total. Then, unit efficacy of this experiment was shown as 0.45 cm^3 necrosed tumor volume from one injection site by once irradiation using 1,037 J in once alone (**Figure 8**). This value derived from rat MAT-LyLu tumor

experiment was definitely very preliminary, but notably did work as a benchmark in rat DMBA tumors.

The value of unit efficacy was only available under the standard treatment condition which was specified by magnetic flux density; 15 mT, magnetic field frequency; 100 kHz, injected amount of MCL particles; 45 mg, irradiation duration; 30 min and generated heating value of 1,037 J in once alone. When amount of MCL particles was lower than 45 mg, due to low concentration of liquid formulation and/or tolerable injection duration of patients, unit efficacy declined proportionally to heat dose index. Actually, 7.5 mg MCL particles was injected to construct partially necrosed tumor sample (**Figure 4a**). In low range of injected MCL particles, compensation of heat dose by boosting irradiation conditions did not guarantee unit efficacy. To our knowledge and experience, magnetic flux density over 15 mT, irradiation duration over 30 min and irradiation times over thrice were unnecessary or unpractical for clinical application.

5. Novel principle of the therapy

The therapy with functionalized heat-generating nanoparticles named MCL particles was based on Gilchrist's idea to use heat-generating material in combination with external energy irradiator [5,6] and was enabled by modern nanotechnology to manipulate and analyze nanoscale substances. As Gordon had suggested significance of biophysical properties of nano-materials [11], composite structure of MCL particles with lipids components have matched to confer several functions such as cell-adhesion activity (**Figure 2**), mobility *in vivo* for necrosis expansion (**Figure 3,4**), stability and reusage in the multiple irradiation protocol (**Figure 2,3,4,9**) and none infiltration properties to normal tissue (**Figure 6**).

As a result, heating region of cancer patient was delimited within tumor tissue. Heating value needed for 1.36 cm^3 tumor regression was shown as 3,111 J in thrice total and was estimated thousands folds less than that of conventional regional heating devises at least [1-3] (**Figure 1a**). Novel fashion of necrosed area expansion *in vivo* was enabled by mobility of heat-generating nanoparticles, which was clearly out of scope of heating-implants fixed in tumor tissue (**Figure 1b**). Mobility of heat-generating nanoparticles provided opportunity to access tumor cells in every corner of tumor tissue (**Figure 1c,d**).

Number of MCL particles in the standard injection amount of 45 mg (containing 26 mg magnetite (Fe_3O_4)) can be calculated with magnetites physical properties; cubic structure, 10 nm average size, 5.17 g/cm^3 density and averagely 25 containments. The answer is hundred-trillion particles. Novelty of the therapy will be clarified by imaging that hundred-trillion of MCL particles in virus size of 100 nm attacked billons of cancer cells in 1 cm^3 tumor volume with moving in tumor tissue and generating thousands of Joules, and killed in a fashion of like nano-thermal ablation (**Figure 1c,d**).

6. Advantage of the therapy

Complete regression of transplanted tumors has been reported with allogenic models of 6 kinds of cancers from 4 kinds of animal species, and with nude-mouse models of human prostate and breast cancers [21] (p.121), [26]. Complete regression was also reported in naturally emerging melanoma of *ret* transgenic mouse model [20] and chemical carcinogen DMBA induced rat mammary tumor model [27]. In clinical research, human follicular thyroid was completely regressed under sufficient heat dose condition achieved contingently [22] (p.1721), [29] (p.26).

Reason for these so frequent and wide-range complete regressions can be given by multiple actions such as primary tumor necrosed induction, anticancer immune induction, tumor cell starvation and accessibility to every corner of destructing tumor tissue, so far revealed. It is notable that these actions consisted of rather general elements such as charge-dependent targeting to cancer cells [45], thermodynamic destruction of

cellular and blood vessel structures, and innate thrombosis and immune system. Advantage of the therapy was considered to be broad availability in human cancers and safety. Adverse events of the therapy were not observed including clinical research [21], [22] (p.1721). Toxicity of MCL particles alone was not observed in preclinical study using rats and dogs including intravenous injection (**unpublished result**).

7. Feasibility of clinical operations and target cancers of the therapy

Magnetites in about 10 nm could be manufactured by the common method reported, and clinically applicable cationic lipid of 1,2-dioleoyl-3-trimethylammonium-propane chloride [46] was available instead of originally used N-(α-trimethyl-ammonio-acetyl)-didodecyl-D-glutamate chloride [15,24]. Large scale manufacturing of MCL particles with weighable magnetites granules has been established [47]. Liquid formulation of MCL particles could be specified by two major items of zeta potential and heat generating activity [24]. AMF irradiators to achieve magnetic flux density of 15 mT at tumor locus have been reported as ferrite core inserted solenoid type [21] (p.124), [26,48] and transverse type of MFH300F with 300 mm gap [49]. These two types have been clinically applied to skin closed cancers [22] (p.1721) and deep-seated cancers [50] respectively. Quality control of two medical devices is critical to guarantee heat dose index.

Intratumor injection should be done slowly with syringe pump, preferably at the standard injection speed of 0.1 ml/10 min. In human prostate tumor, 0.5 ml of liquid formulation has been successfully injected by 30 min pumping [51]. Computerized tomography X ray imaging has been clinically used to monitor core magnetites [50,51]. Additional targeted injection into undistributed tumor area and following irradiations will be considerable as reported in animal tumor model [19]. Necessity of anesthesia was not always concluded, since some clinical cases of skin closed melanoma were treated properly without anesthesia (**unpublished results**). Invasive temperature monitoring [52] is not essential in this therapy.

Clinical benefits of the therapy are considered low physical burden, early response and safety so far. The therapy will be beneficial for patients in low performance status and in exhaustion of current therapies. The therapy will be applicable to inoperatable cancers due to risky neighboring tissue or organ in combination with X ray monitoring. Neoadjuvant use for surgery and combination use with immune check point inhibitors or chemotherapeutic agents will be practical. Extremely small, large or sclerotic tumors will be not eligible because of injection difficulty. Further clinical developments should be conducted with accurately-specified MCL particles and AMF irradiators in consideration of the principle, advantage and limitation of the therapy.

Acknowledgment: We would like to express sincere thanks to Masashige Shinkai, Hiroyuki Honda, Toshiyuki Hakata, Syota Tanoue, Syuichiro Miyata, Kotaro Hirayama, Jun Motoyama, Noriyuki Yamashita, Hiroshi Takase, Kazuhiko Matsumoto, Toshiaki Saida, Ichiro Ono, Jimbow Kowichi, Takashi Nagai, Toshiki Etani, Taku Naiki, Kohri Kenjiro, Toshihiko Wakabayashi, Jun Yoshida, Tsuneo Imai, Toyone Kikumori, Yoshihiro Nishida, Noriyuki Yamamoto for their technical, scientifical or clinical contributions.

Conflict of Interest: The authors declare no potential conflict of interest.

References

[1] Storm K., Baker H., Scanlon E., Plenk H., Meadows P., Cohen S., Olson C., Thomson J., Khandekar J., Roe D., Nizze A., Morton D. Magnetic-induction hyperthermia. Results of a 5-years multi-institutional national cooperative trial in advanced patients. *Cancer* **1985**, 55: 2677-2687. DOI: 10.1002/1097-0142(19850601)55:11<2677::aid-cncr2820551124>3.0.co;2-o

[2] Abe M., Hiraoka M., Takahashi M., Egawa S., Matsuda C., Onoyama Y., Morita K., Kakehi M., Sugawara T. Multi-institutional studies on hyperthermia using an 8-MHz radiofrequency capacitive heating device (Thermotron RF-8) in

combination with radiation for cancer therapy. *Cancer* **1986**, 58: 1589-1595. DOI: 10.1002/1097-0142(19861015)58:8<1589::aid-cncr2820580802>3.0.co;2-b

[3] Sapozink M., Gibbs F., Egger M., Stewart J. Abdominal regional hyperthermia with an annular phased array. *J Clin Oncol* **1986**, 4: 775-783. DOI: 10.1200/JCO.1986.4.5.775

[4] Madersbacher S., Pedevilla M., Vingers L., Susani M., Marberger M. Effect of high-intensity focused ultrasound on human prostate cancer *in vivo*. *Cancer Res* **1995**, 55: 3346-3351

[5] Gilchrist R., Medal R., Shorey W., Hanselman R., Parrott J., Taylor B. Selective inductive heating of lymph nodes. *Ann Surg* **1957**, 141: 596-606. DOI: 10.1097/00000658-195710000-00007

[6] Gilchrist R., Shorey W., Hanselman R., DePeyster F., Yang J., Medal R. Effects of electromagnetic heating on in viscera: A preliminary to the treatment of human tumors. *Ann Surg* **1965**, 161: 890-896. DOI: 10.1097/00000658-196506000-00008

[7] Tohnai I., Goto Y., Hayashi Y., Kaneda T., Kobayashi T., Kida Y., Matsui M. Interstitial hyperthermia for cancer of the tongue using an implant heating system. *Jpn J Hyperthermic Oncol* **1990**, 6: 450-461. DOI: 10.3191/thermalmedicine.6.439

[8] Berthusen H, Tucker D, Park B. A field-focusing device to increase power output of ThermoRod trade mark implants for thermal ablation of tissue. *J Biomed Mater Res* **2002**, 63: 650-656. DOI: 10.1002/jbm.10385

[9] Matsumine A., Kusuzaki K., Matsubara T., Shintani K., Satonaka H., Wakabayashi T., Miyazaki S., Morita K., Takegami K., Uchida A. Novel hyperthermia for metastatic bone tumors with magnetic materials by generating an alternating electromag-netic field. *Clin Exp Metastasis* **2007**, 24: 191-200. DOI: 10.1007/s10585-007-9068-8

[10] Wood B., Ramkaransingh J., Fijo T., Walther M., Libutti S. Percutaneous tumor ablation with radiofrequency. *Cancer* **2002**, 94(2): 443-451. DOI: 10.1002/cncr.10234

[11] Gordon R. T., Hines J., Gordon D. Intracellular hyperthermia, A biophysical approach to cancer treatment via intracellular temperature and biophysical alteration. *Med Hypothesis* **1979**, 5: 83-102. DOI: 10.1016/0306-9877(79)90063-x

[12] Jordan A., Wust P., Fahling H., John W., Hinz A., Felix R. Inductive heating of ferromagnetic particles and magnetic fluids: physical evaluation and their potential for hyperthermia. *Int J Hyperthermia* **1993**, 9: 51-68. DOI: 10.3109/02656739309061478

[13] Mitsumori M., Hiraoka M., Shibata T., Okuno Y., Masunaga S., Koishi M., Okajima K., Nagata Y., Nishimura Y., Abe M., Ohura K., Hasegawa M., Nagae H., Ebisawa Y. Development of intra-arterial hyperthermia using a dextran-magnetite complex. *Int J Hyperthermia* **1994**, 10: 785-793. DOI: 10.3109/02656739409012371

[14] Kolosnjaj-Tabi J., Corato R., Lartigue L., Iris M., Guardia P., Silva A. Amanda, Luciani N., Clement O., Flaud P., Singh J., Decuzzi P., Pellegrino T., Wilhelm C., Gazeau F. Heat-generating iron oxide nanocubes: subtle "destructurators" of the tumoral microenvironment. *ACSNano* **2014**, 8: 4268-4283. DOI: 10.1021/nn405356r

[15] Shinkai M., Yanase M., Honda H., Wakabayashi T., Yoshida J., Kobayashi T. Intracellular hyperthermia for cancer using magnetite cationic liposomes: *In vitro* study. *Jpn J Cancer Res* **1996**, 87: 1179-1183. DOI: 10.1111/j.1349-7006.1996.tb03129.x

[16] Yanase M., Shinkai M., Honda H., Wakabayashi T., Yoshida J., Kobayashi T. Intracellular hyperthermia for cancer using magnetite cationic liposomes: An *in vivo* study. *Jpn J of Cancer Res* **1998**, 89: 463-469. DOI: 10.1111/j.1349-7006.1998.tb00586.x

[17] Matsuno H., Tohnai I., Mitsudo K., Hayashi Y., Ito M., Shinkai M., Kobayashi T., Yoshida J., Ueda M. Interstitial hyperthermia using magnetite cationic liposomes inhibit to tumor growth of VX-7 transplanted tumor in rabbit tongue. *Jpn J Hyperthermic Oncol* **2001**, 17: 141-149. DOI: 10.3191/thermalmedicine.17.141

[18] Ito A., Shinkai M., Honda H., Yoshikawa K., Saga S., Wakabayashi T., Yoshida J., Kobayashi T. Heat shock protein 70 expression induces an antitumor immunity during intracellular hyperthermia using magnetite nanoparticles. *Cancer Immunol Immunother* **2003**, 52: 80-88. DOI: 10.1007/s00262-002-0335-x

[19] Ito A., Tanaka K., Honda H., Abe S., Yamaguchi H., Kobayashi T. Complete regression of mouse mammary carcinoma with a size greater than 15 mm by frequent repeated hyperthermia using magnetite nanoparticles. *J Biosci Bioeng* **2003**, 96: 364-369. DOI: 10.1016/S1389-1723(03)90138-1

[20] Ito A., Nakahara Y., Fujioka M., Kobayashi T., Takeda K., Nakashima I., Honda H. Complete regression of hereditary melanoma in a mouse model by repeated hyperthermia using magnetite cationic liposomes. *Thermal Med* **2005**, 21: 139-149. DOI: 10.3191/thermalmedicine.21.139

[21] Ito A., Kobayashi T.: Intracellular hyperthermia using magnetic nanoparticles: A novel method for hyperthermia clinical applications. *Thermal Med* **2008**, 24: 113-129. DOI: 10.3191/thermalmed.24.113

[22] Kobayashi T., Kakimi K., Nakayama E., Jombow K. Antitumor immunity by magnetic nanoparticle-mediated hyperthermia. *Nanomedicine* **2014**, 9: 1715-1726. DOI: 10.2217/nnm.14.106

[23] Motoyama J., Hakata T., Kato R., Yamashita N., Morino T., Kobayashi T., Honda H. Size dependent heat generation of magnetite nanoparticles under AC magnetic field for cancer therapy. *BioMag Res Tech* **2008**, 6: e4. DOI: 10.1186/1477-044X-6-4

[24] Morino T., Takase H., Etani T., Naiki T., Kawai N., Ito A., Yasui T. Medium temperature independent cytotoxicity of cell-adhesive heat-generating nanoparticles named magnetite cationic liposomes and its therapeutic use. *Thermal Med* **2020**, 36: 25-34. DOI: 10.3191/thermalmed.36.25

[25] Morino T., Takase H., Kawai N., Nagai T., Etani T., Naiki T., Yasui T. Mode of tumor necrosis induction *in vivo* by heat-generating nanoparticles of magnetite cationic lipid composite particles dispersing toward neighbor naïve tumor zone and its therapeutic use. *Thermal Med* **2022**, 38: 19-26. DOI: 10.3191/thermalmed.38.19

[26] Morino T., Tanoue S., Miyata S., Hirayama K., Ito A., Etani T., Naiki T., Kawai N., Yasui T. Heat dose index *in vivo* for cancer therapy using heat-generating nanoparticles named magnetite cationic liposomes and alternating magnetic field irradiator. *Thermal Med* **2020**, 36: 47-58. DOI: 10.3191/thermalmed.36.47

[27] Morino T., Ito A., Etani T., Naiki T., Kawai N., Yasui T. Heat dose based large tumor treatment with multiple site injections of heat-generating nanoparticles dispersible within tumor tissue. *Thermal Med* **2020**, 36: 91-98. DOI: 10.3191/thermalmed.36.101

[28] Creixell M., Bohórquez A., Torres-Lugo M., Rinaldi C. EGFR-targeted magnetic nanoparticles heaters kill cells without a perceptible temperature rise. *ACSNano* **2011**, 5: 7124-7129. DOI: 10.1021/nn201822b

[29] Morino T., Etani T., Naiki T., Kawai N., Kikumori T., Nishida Y., Yamamoto N., Yasui T. Outcome of cancer clinical researches using heat-generating nanoparticles and novel concept of its therapeutic use. *Thermal Med*, **2019**, 35: 23-32. DOI: 10.3191/thermalmed.35.23

[30] Boucher Y., Brekkent C., Netti A., Baxter T., Jain K. Intratumoral infusion of fluid: Estimation of hydraulic conductivity and implications for the delivery of therapeutic agents. *Br J Cancer* **1998**, 78: 1442-1448. DOI: 10.1038/bjc.1998.705

[31] Welter M., Rieger H. Interstitial fluid flow and drug delivery in vascularized tumors: A computational model. *PLoS One* **2013**, 8: e70395. DOI: 10.1371/journal.pone.0070395

[32] Baluk P., Morikawa S., Haskell A., Mancuso M., McDonald D. Abnormalities of basement membrane on blood vessels and endothelial sprouts in tumors. *Am J Pathol* **2003**, 163: 1801-1815. DOI: 10.1016/S0002-9440(10)63540-7

[33] Hori K., Saito S. Microvascular mechanisms by which the combretastatin A-4 derivative AC7700 [AVE8062] induces tumour blood flow stasis. *Br J Cancer* **2003**, 89: 1334-1344. DOI: 10.1038/sj.bjc.6601261

[34] Yanase M., Shinkai M., Honda H., Wakabayashi T., Yoshida J., Kobayashi T. Antitumor immunity induction by intracellular hyperthermia using magnetic cationic liposomes. *Jpn J Caner Res* **1998**, 89: 775-782. DOI: 10.1111/j.1349-7006.1998.tb03283.x

[35] Shido Y., Nishida Y., Suzuki Y., Kobayashi T., Ishiguro N. Targeted hyperthermia using magnetite cationic liposomes and an alternating magnetic field in a mouse osteosarcoma model. *J Bone Joint Surg Br* **2010**, 92: 580-585. DOI: 10.1302/0301-620X.92B4.22814

[36] Matsumura, Y. and Maeda, H. A new concept for macromolecular therapeutics in cancer chemotherapy: mechanism of tumoritropic accumulation of proteins and the antitumor agent SMANCS. *Cancer Res* **1986**, 46: 6387-6392.

[37] Tomimatsu M. Electron microscopic observation of human hepatocellular carcinoma. A comparative study of ultrastructures of four different histological patterns [trabecular, compact, pseudoglandular and scirrhous patterns]. Kanzo **1987**, 28: 76-83.

[38] Lieleg O., Baumgarte R., Bausch A. Selective filtering of particles by the extracellular matrix: An electrostatic bandpass. *Biophys J* **2009**, 97: 1569-1577. DOI: 10.1016/j.bpj.2009.07.009

[39] Ferrell N., Groszek J., Li L., Smith R., Butler R., Zorman C, Roy S., Fissell W. Basal lamina secreted by MDCK cells has size- and charge-selective properties. *Am J Physiol Renal Physiol* **2011**, 300: F86-F90. DOI: 10.1152/ajprenal.00484.2010

[40] Vllasaliua D., Falconeb H. F., Stolnika S., Garnetta M. Basement membrane influences intestinal epithelial cell growth and presents a barrier to the movement of macromolecules. *Exp Cell Res* **2014**, 323: 218-231. DOI: 10.1016/j.yexcr.2014.02.022

[41] Miner J. Glomerular basement membrane composition and the filtration barrier. *Pediatr Nephrol* **2011**, 26: 1413-1417. DOI: 10.1007/s00467-011-1785-1

[42] Strohbehn J. Calculation of absorbed power in tissue for various hyperthermia devices. *Cancer Res* **1984**, 44: 4781s-4787s

[43] Dewhirst M., Sim D. The utility of thermal dose as a predictor of tumor and normal tissue responses to combined radiation and hyperthermia. *Cancer Res* **1984**, 44: 4772s-4780s.

[44] Maguire P., Samulski T., Prosnitz L., Jones E., Rosner G., Powers B., Layfield L., Brizel D., Scully S., Harrelson J., Dewhirst M. A phase II trial testing the thermal dose parameter CEM43 degrees T90 as a predictor of response in soft tissue sarcomas treated with pre-operative thermoradiotherapy. *Int J Hyperthermia* **2001**, 17: 283-290. DOI: 10.1080/02656730110039449

[45] Marquez M., Nilsson S., Lennartsson L., Liu Z., Tammela T., Raitanen M., Holmberg R. A. Charge-dependent targeting: results in six tumor cell lines. *Anticancer Res* **2004**, 24: 1347-1351.

[46] Porteous J., Dorin R., Davidson-Smith H., Davidson H., Stevenson J., Carothers D., Wallace H., Moralee S., Hones C, Kallmeyer G., Michaelis U., Naujoks K., Ho L-P, Samways M., Greening P., Innes A. Evidence for safety and efficacy of DOTAP cationic liposome mediated CFTR transfer to the nasal epithelium with cystic fibrosis. *Gene Therapy* **1997**, 4: 210-218. DOI: 10.1038/sj.gt.3300390

[47] Patent in preparation. Magnetic field responding heat generating materials for thermal therapy, its liquid formulation and its manufacturing method.

[48] Kawai N., Ito A., Nakahara Y., Honda H., Kobayashi T., Futakuchi M., Shirai T., Tozawa K., Kohri K. Complete regression of experimental prostate cancer in nude mice by repeated hyperthermia using magnetite cationic liposomes and a newly developed solenoid containing a ferrite core. *Prostate* **2006**, 66: 718-727. DOI: 10.1002/pros.20394

[49] Gneveckow U., Jordan A., Scholz R., Bruss V., Waldofner N., Ricke J., Feussner A., Hildebrandt B., Rau B., Wust P. Description and characterization of the novel hyperthermia-and thermoablation-system MFH300F for clinical magnetic fluid hyperthermia. *Med Phys* **2004**, 31: 1444-1451. DOI: 10.1118/1.1748629

[50] Johannsen M., Gneveckow U., Eckelt L., Feussner A., WaldÖFner N., Scholz R., Deger S., Wust P., Loening S., Jordan A. Clinical hyperthermia of prostate cancer using magnetic nanoparticles: Presentation of a new interstitial technique. *Int J Hyperthermia* **2005,** 21: 637-647. DOI: 10.1080/02656730500158360

[51] Kawai N., Kobayashi T., Kobayashi D., Tsutsumiuchi K., Iida K., Etani T., Naiki T., Ando R., Mizuno K., Okada A., Tozawa K., Yasui T. Safety of regional 8-MHz radiofrequency capacitive hyperthermia combined with magnetic cationic liposomes in patients with castration–resistant prostate cancer: A Phase 1 clinical study. *J Int Transl Med* **2016**, 4: 258-267. Doi: 10.11910/2227-6394.2016.04.04.07

[52] Fessenden P., Lee E., Samulski T. Direct temperature measurement. *Cancer Res* **1984**, 44: 4799s-4804s.